JOURNAL OF SYNCHROTRON RADIATION
ISSN 1600-5775

Three-dimensional visualization of fibrous tissues in cirrhotic rats via X-ray phase-contrast computed tomography with iodine staining

Jianbo Jian,[a,b]‡ Xinyan Zhao,[c]‡ Lili Qin,[a] Yuqing Zhao,[a] Mengyu Sun,[a] Wenjuan Lv[a] and Chunhong Hu[a]*

[a]College of Biomedical Engineering, Tianjin Medical University, Tianjin 300070, People's Republic of China, [b]Department of Radiation Oncology, Tianjin Medical University General Hospital, Tianjin 300052, People's Republic of China, and [c]Liver Research Center, Beijing Friendship Hospital, Capital Medical University, Beijing 100050, People's Republic of China. *Correspondence e-mail: chunhong_hu@hotmail.com

Received 18 December 2018
Accepted 30 April 2019

Edited by S. Svensson, Uppsala University, Sweden

‡ These authors contributed equally to this work.

Keywords: X-ray phase-contrast computed tomography; cirrhosis; fibrous tissues; iodine staining; three-dimensional imaging.

Supporting information: this article has supporting information at journals.iucr.org/s

To accurately characterize cirrhosis, knowledge of the 3D fibrous structures is essential. Histology is the gold standard in cirrhosis screening, but it mainly provides structural information in 2D planes and destroys the 3D samples in the process. The aim of this study was to evaluate the potential of X-ray phase-contrast computed tomography (PCCT) with iodine staining for the 3D nondestructive visualization of internal structural details in entire cirrhotic livers with histopathologic correlation. In this study, cirrhotic livers induced by carbon tetrachloride (CCl_4) in rats were imaged via PCCT and then histopathologically processed. Characteristics of the cirrhosis, *i.e.* abnormal nodules surrounded by annular fibrosis, were established and a 3D reconstruction of these structures was also performed via PCCT. Fibrosis area, septal width and nodular size were measured and the correlation for these quantitative measurements between PCCT and histopathologic findings was analyzed. The results showed that fibrous bands, small nodules and angio-architecture in cirrhosis were clearly presented in the PCCT images, with histopathologic findings as standard reference. In comparison with histopathology, PCCT was associated with a very close value for fibrosis area, septal width and nodular size. The quantitative measurements showed a strong correlation between PCCT and histopathology. Additionally, the 3D structures of fibrous bands and microvasculature were presented simultaneously. PCCT provides excellent results in the assessment of cirrhosis characteristics and 3D presentation of these feature structures compared with histopathology. Thus, the technique may serve as an adjunct nondestructive 3D modality for cirrhosis characterization.

1. Introduction

Cirrhosis is a diffuse process characterized by fibrosis and the conversion of normal liver architecture into structurally abnormal nodules surrounded by annular fibrosis (Anthony *et al.*, 1978; Soresi, 2014). The morphological changes result in increased resistance to portal blood flow and hence in portal hypertension which causes most deaths in cirrhotic patients (Thabut & Shah, 2010; Cárdenas & Ginès, 2009). Histopathology can directly provide information regarding the morphological changes and is regarded as the gold standard for evaluating the extent of cirrhosis. However, this approach has two major limitations. Firstly, it is a time-consuming, complex and destructive process, which prohibits further analysis with other methods. Secondly, histopathology mainly provides 2D slices at given angles, often yielding discontinuous and incomplete information. Although 3D volume can be obtained by 3D reconstruction of serial histological sections,

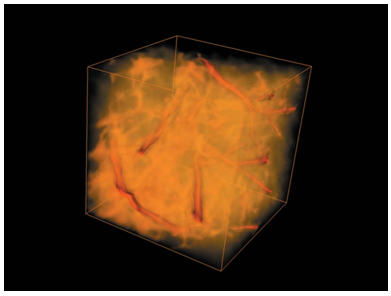

this method holds limitations and requires specialists (Gerneke *et al.*, 2007; Mohun & Weninger, 2011; Ourselin *et al.*, 2001). A 3D analysis of whole specimens is crucial for accurate characterization of the cirrhosis. Thus, a 3D nondestructive imaging method to image the cirrhosis is desirable.

Several nondestructive imaging techniques have been used in assessing cirrhosis. Computed tomography (CT) provides direct anatomical information within samples, but has difficulty in distinguishing soft tissues (Holdsworth & Thornton, 2002). Although this limitation can be partly overcome by the injection of a contrast agent, imaging fibrous tissues remains challenging. On the contrary, magnetic resonance imaging (MRI) provides superior soft-tissue contrast compared with CT at the cost of reduced spatial resolution and longer acquisition times. Optical techniques such as optical coherence tomography (OCT) feature high spatial resolution (on the order of several micrometres or nanometres), offer excellent soft-tissue contrast and even allow *in vivo* imaging, but the main limitation is penetration depth which makes whole-organ imaging difficult (Ntziachristos, 2010).

X-ray phase-contrast computed tomography (PCCT) is an emerging imaging modality that utilizes the phase shift of X-rays passing through matter to generate tissue contrast, as opposed to conventional X-ray imaging that uses the X-ray attenuation as the imaging signal (Momose, 2005; Fitzgerald, 2000). Early studies have demonstrated that PCCT has a superior image contrast in biological soft tissues than conventional imaging modalities such as CT or MRI (Geith *et al.*, 2018; Winklhofer *et al.*, 2015; Hu *et al.*, 2017). Recent experiments have suggested that PCCT could clearly reveal the abnormal angio-architecture of the fibrotic liver in small-animal models (Duan *et al.*, 2013; Xuan *et al.*, 2015). However, evidence for the potential benefits of PCCT in imaging fibrous bands and small nodules in the cirrhotic liver remains scarce. Some studies have reported that sample staining with iodine would enable PCCT to yield a higher contrast in imaging fibrous tissues (Jiang *et al.*, 2014, 2012), which might provide a new means of revealing fibrous tissues in the cirrhotic liver.

The present work evaluates the potential of PCCT with iodine staining for the characterization of cirrhosis in small animal models. We hypothesized that (i) cirrhosis sample staining with iodine enables PCCT to yield a higher contrast in imaging fibrous tissues; (ii) important cirrhotic characters, *i.e.* fibrous bands, small nodules, *etc.*, can be detected, differentiated and quantified by PCCT; and (iii) 3D architectures of the fibrous tissues and microvasculature in cirrhotic liver can be reconstructed and presented simultaneously.

2. Materials and methods

2.1. Sample preparation

All animal experiments were approved by the Institutional Review Board and were carried out in accordance with the guiding principles for care. Male adult Sprague–Dawley rats (n = 24) weighing 180–220 g were maintained in an environmentally controlled room (23 ± 2°C, 55 ± 10% humidity) with a 12 h light/dark cycle and free access to food and water. Cirrhosis was induced via the administration of 2 ml per kg body weight of CCl_4/olive oil (4:6, v/v) by intraperitoneal injection twice per week for up to 12 weeks (Constandinou *et al.*, 2005). The rats were randomly divided into a stained group (six normal and six cirrhotic cases) and an unstained group (six normal and six cirrhotic cases). The livers from all animals were removed after euthanasia and then fixed in neutral phosphate-buffered formalin (10%).

2.2. Soft-tissue staining

Since the discovery of X-rays, X-ray technologies have been widely used for biomedical imaging due to their excellent performance in biomedical tissue imaging. However, current clinical X-ray technologies, mainly relying on X-ray absorption, are very suited for imaging hard-tissues (such as bone) but cannot provide enough image contrast for soft tissues (such as vessels, fibrous tissues) which are low absorbing. Thus, the soft-tissue staining method has been developed to solve the problem of soft-tissue imaging. Soft-tissue staining refers to the *ex vivo* staining of soft tissues with solutions that contain heavy ions such as tungsten, iodine, silver or barium before X-ray imaging (Metscher, 2009*a*). The staining method is mainly related to differences in the diffusion speed between different tissue types (Albers *et al.*, 2018). This approach has recently been used in various types of samples such as mouse embryos, hearts and kidneys (Metscher, 2009*b*; Dullin *et al.*, 2017; Missbach-Guentner *et al.*, 2018). Additionally, PCCT has solved the problem of soft-tissue imaging to a large extent, especially in the field of vascular imaging. However, it is still difficult to clearly distinguish the fibrous tissues in fibrosis/cirrhosis. A previous study has shown that fibrous tissues in liver fibrotic diseases present a fuzzy shadow-like structure in PCCT images, making it difficult for them to be visualized in 3D (Fu *et al.*, 2016). Recently, researchers have used PCCT staining with iodine to successfully reveal the collagen structure in dermal tissue (Jiang *et al.*, 2014, 2012), which provides a new idea for solving fibrous-tissue (mainly composed of collagen) imaging problems in cirrhosis.

After fixation, the livers in the stained group were placed in iodine solution (2% elemental iodine, 2.5% potassium iodide, 50% ethanol and the balance water). The components in the staining solution refer to the previous studies of collagen imaging (Jiang *et al.*, 2014, 2012). The samples were stained with 5 ml of staining solution for 5 days (the livers were moving freely within the sample container) prior to imaging. For stain development and optimization, the staining time from 1 to 7 days was tested (Section S1 of the supporting information). The results showed 5 days was the optimal time in which the liver parenchyma became fully stained and iodine did not diffuse into the fibrous tissues.

2.3. Experimental setup

PCCT experiments were performed at beamline BL13W1 of the Shanghai Synchrotron Radiation Facility (SSRF),

Shanghai, China. The experimental setup described in detail in Xie *et al.* (2013) contains an X-ray source, monochromator, sample stage, detector and image acquisition system. A schematic diagram of the setup and details about the components and parameters are provided in Fig. 1. In the PCCT imaging system, the incident white synchrotron X-ray beam emerging from a 3.5 GeV electron storage ring was monochromated by an Si(111) double-crystal monochromator. The tunable energy range of the X-ray beam was 8–72.5 keV, and was adjusted to 26 keV in this experiment. Subsequently, the monochromatic beam passed through the sample fixed on a rotation stage, and the transmitted beam was recorded by a CCD camera (VHR1:1; Photonic Science Ltd, Robertsbridge, UK) producing a raw projection with an effective pixel size of 9 µm × 9 µm. During the CT data acquisition, a total of 600 raw projections were obtained from each sample over 180° in rotation steps of 0.3°. In addition, 20 flat-field images (with no sample in the beam) and 10 dark-field images (dark signal in the absence of photons) were also collected to correct for the dark current offset of the detector (Weitkamp *et al.*, 2011).

2.4. CT reconstruction and 3D visualization

After the PCCT scanning, the obtained raw projections were first subjected to flat-field and dark-field corrections, and then a phase retrieval method, *i.e.* the phase-attenuation duality Born-type approximation phase retrieval algorithm (PAD-BA) (Chen *et al.*, 2011) was employed to extract phase information from the projections. Subsequently, the phase images that only contained phase information were reconstructed using the filtered back-projection algorithm to build a stack of CT slices. The dark-field correction, phase retrieval and CT reconstruction were processed using the software *PITRE* (Chen *et al.*, 2012), which is a professional software package widely used in PCCT experiments. The 3D reconstruction of the cirrhotic tissues was performed with *Avizo Fire 8.0* (FEI Visualization Sciences Group), which allowed a clear visualization of the complex spatial relationships between anatomical features. The complete process was described in detail in Section S2 of the supporting information.

2.5. Histological analysis

After imaging, the samples were dehydrated and embedded in paraffin. Serial sections with a slice thickness of 4 µm were taken and stained with Sirius Red to observe the fibrous tissues. Images were digitized using a dedicated camera and an image analysis was performed using *Image-Pro Plus 6.0* software (Media Cybernetics, Bethesda, Maryland, USA). Fibrosis area, septal width and nodular size on the histological images were calculated by a pathologist (with ten years of experience in liver pathology) who was blinded to the findings on the PCCT images. Details about the quantitative measurements can be found in Section S3 of the supporting information.

2.6. PCCT image analysis

The fibrous tissues and small nodules were identified and marked in the PCCT sections by using the histological slices as the reference. For quantitative analysis, co-registration of the PCCT images and the corresponding histopathologic findings is a necessary step. Anatomical landmarks, such as the lumen shape, nodular size and morphologic features of the fibrous band, were used to match the PCCT images and histopathological slices. Then, similar to histopathological findings, fibrosis area, septal width and nodular size on the PCCT images were performed by two radiologists (with more than five years of experience in liver imaging) who were blinded to the histopathologic results.

2.7. Statistical data analysis

Statistical analysis was performed using *SPSS* 19.0 software (IBM, Chicago, IL, USA). Numerical results are presented as the means ± standard deviations. The correlation between the histopathological findings and PCCT quantitative measurements was analyzed by the Pearson correlation coefficient R.

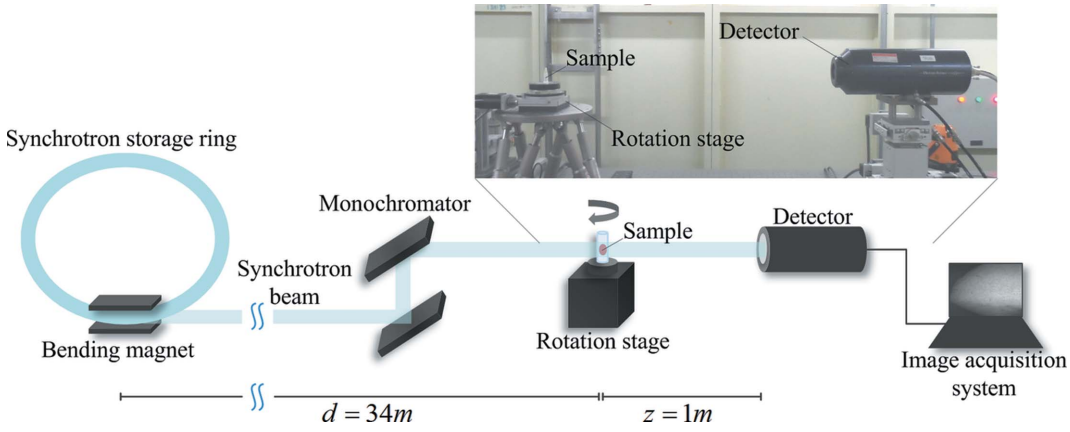

Figure 1
Schematic diagram of the experimental setup. Parallel X-rays are derived from a 3.5 GeV electron storage ring and are monochromated by a double-crystal monochromator with Si(111) crystals. The beam is projected on the sample fixed on a rotation stage, and the transmitted beam is recorded by an image detector. Finally, the projection images of the sample are displayed via the image acquisition system.

A P value of less than 0.05 was considered to be statistically significant.

3. Results

3.1. Comparisons of PCCT images with and without staining

Cirrhotic rat livers in stained and unstained groups were imaged with PCCT. As expected, anatomical structural information in the unstained liver was not clearly visible [Fig. 2(*a*)]. After staining, the overview PCCT scan provided a clear distinction of the different anatomical structures, such as fibrous bands, small nodules and vessels [Fig. 2(*b*)]. The remarkable contrast enhancement compared with the unstained cirrhotic liver is further seen in the line profile of the PCCT images [Figs. 2(*c*) and 2(*d*)]. This study used iodine for staining soft tissues, thereby generating a strongly negative contrast for the fibrous tissues and allowing for their visualization in the cirrhotic liver.

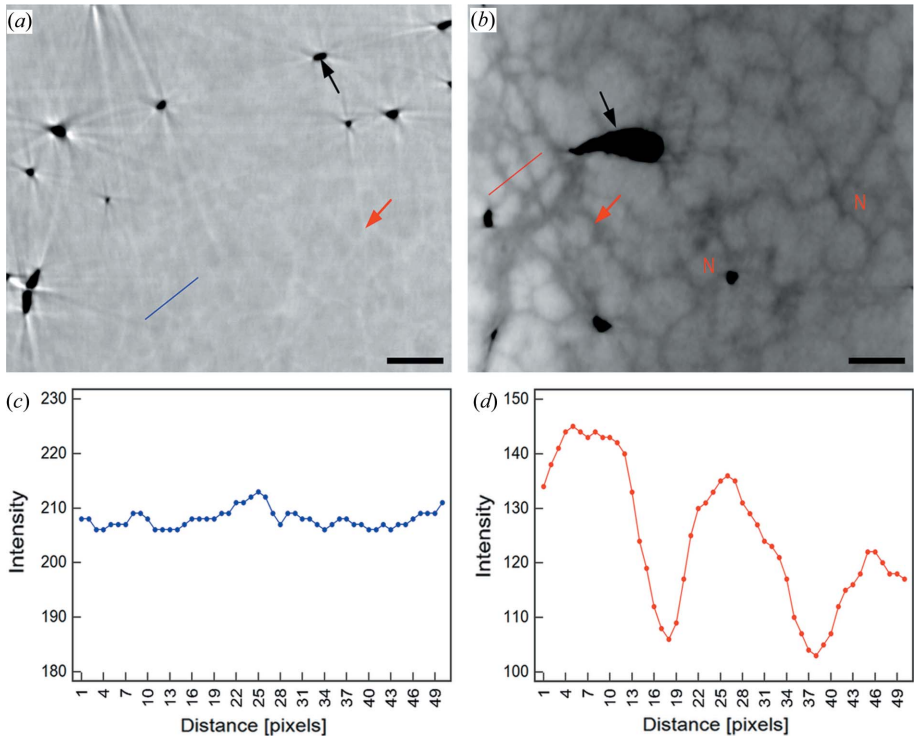

Figure 2
PCCT slices of unstained and stained cirrhotic livers and the corresponding line profiles highlighting the contrast enhancement obtained after application of the iodine-based staining protocol. (*a*) Overview image of the unstained cirrhotic liver. (*b*) Overview image of the cirrhotic liver after staining. The following anatomic structural regions could be identified and were labelled: vessel lumens (black arrows) and abnormal nodules (N) surrounded by annular fibrosis (red arrows). (*c*) Profile of the blue line shown in (*a*). (*d*) Profile of the red line shown in (*b*). Scale bar = 500 µm. Window settings have been optimized for both the unstained and stained CT images to provide the best contrast for the fibrous tissues. The improved contrast of the stained PCCT in comparison with that of the unstained PCCT images can be appreciated.

3.2. Comparisons between histological sections and PCCT images

PCCT images of the normal and cirrhotic livers in the stained group with corresponding histological sections are shown in Fig. 3. In the normal liver [Figs. 3(*a*) and 3(*b*)], fibrous tissues are detected in low amounts around the portal tracts and hepatic veins, whereas in the cirrhotic liver [Figs. 3(*c*) and 3(*d*)] the entire liver parenchyma is subdivided into small nodules of varying sizes by fibrous septa, and pseudo-lobules had formed. Due to the iodine contrast, the fibrous septa appear darker compared with the surrounding liver parenchyma. The histopathological findings confirmed the accuracy of the PCCT which provided similar morphological information to the histological slices. To further assess the potential of PCCT in quantifying cirrhosis, quantitative measurements including fibrosis area, septal width and nodular size were analyzed (Table 1). Absolute values of the measurements in PCCT images were very close to these in histopathologic findings, and excellent positive correlations with respect to all analyzed parameters were found ($R \geq 0.928$).

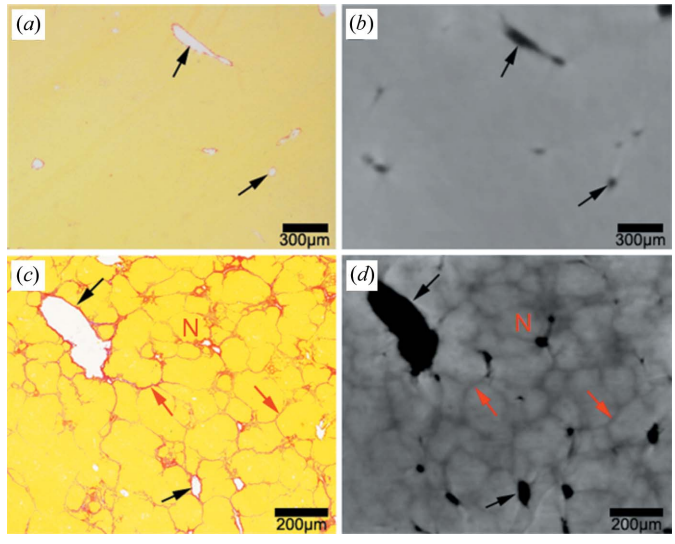

Figure 3
Comparisons between histological sections and PCCT images. Histopathological sections of (*a*) a normal liver and (*c*) a cirrhotic liver stained with Sirius Red. The corresponding PCCT images of the same (*b*) normal liver and (*d*) cirrhotic liver. Microvasculature (black arrows), fibrous septa (red arrows) and small nodules (N) are clearly visualized using PCCT.

3.3. 3D visualization of fibrous tissues in an entire cirrhotic liver

The enormous potential of this method lies in 3D visualization, which has been demonstrated in Fig. 4. The microvessels were clearly shown in the CT slice of an entire liver without any obvious abnormalities [Fig. 4(*a*)], but in the 3D image irregular and tortuous vasculature with numerous

Table 1
Quantitative measurements of fibrous tissues with PCCT in comparison with histopathologic analysis.

Data are based on 30 PCCT images and the corresponding histological sections.

	Measurements			
Parameter	PCCT	Histopathologic analysis	*P* value	Pearson *R*
Fibrosis area (%)	12.1 ± 1.2	12.6 ± 1.3	<0.0001	0.928
Septal width (μm)	26.5 ± 6.3	26.5 ± 7.0	<0.0001	0.975
Nodular size (μm^2)	(6.5 ± 4.9) × 10^4	(6.7 ± 5.3) × 10^4	<0.0001	0.995

branches was observed [Fig. 4(*b*)]. The fibrous septa and pseudo-lobules were also clearly visualized in the CT image, giving a 'mesh' appearance [Fig. 4(*a*)], whereas the fibrous septa connected to each other in the 3D model, appearing honeycomb-like [Fig. 4(*e*)]. Based on the iodine staining method, 3D architectures of the fibrous tissues and microvasculature in the cirrhotic liver were presented simultaneously [Fig. 4(*d*)], showing that dense fibrous tissues aggregated around the vessel walls.

4. Discussion

The present study indicates that PCCT with iodine staining yields a higher image contrast in imaging fibrosis structures compared with the PCCT without staining. By combining iodine staining and specific settings of the synchrotron beamline, typical cirrhosis characteristics, that is, densely distributed pseudo-lobular structures and small nodules of varying sizes, can be clearly distinguished in PCCT images, which is confirmed by the corresponding histopathological findings. A 3D visualization of the fibrous network and microvasculature is presented simultaneously in this study. In addition, the quantitative measurements of the fibrous tissues and small nodules obtained using PCCT show excellent correlation with histopathologic results.

To understand cirrhosis progression, integrating information about the key features and their spatial organization is essential, which requires detailed whole liver 3D morphology at a resolution including all relevant details. However, detecting all these features of cirrhosis, especially in the whole liver, is still a major challenge. Histology/microscopy provides sufficient detail, but hardly allows imaging of the whole liver, and the sectioning destroys the 3D structural integrity of the liver specimen and provides only 2D images. Although it is possible to obtain 3D information, this method has limitations relating to the 2D nature of histology and the deformation caused during processing (Ourselin *et al.*, 2001). Recently, nonlinear optical microscopy imaging techniques, such as second harmonic generation (SHG), coherent anti-Stokes Raman scattering (CARS) or their merged systems (such as qFibrosis), which possess many attractive features such as 3D sectioning capability at submicrometer-scale resolutions, have been used, but whole organ imaging is limited by the penetration depth, one of the well known limitations of these techniques (Sun *et al.*, 2010; He *et al.*, 2010; Lin *et al.*, 2011; Xu

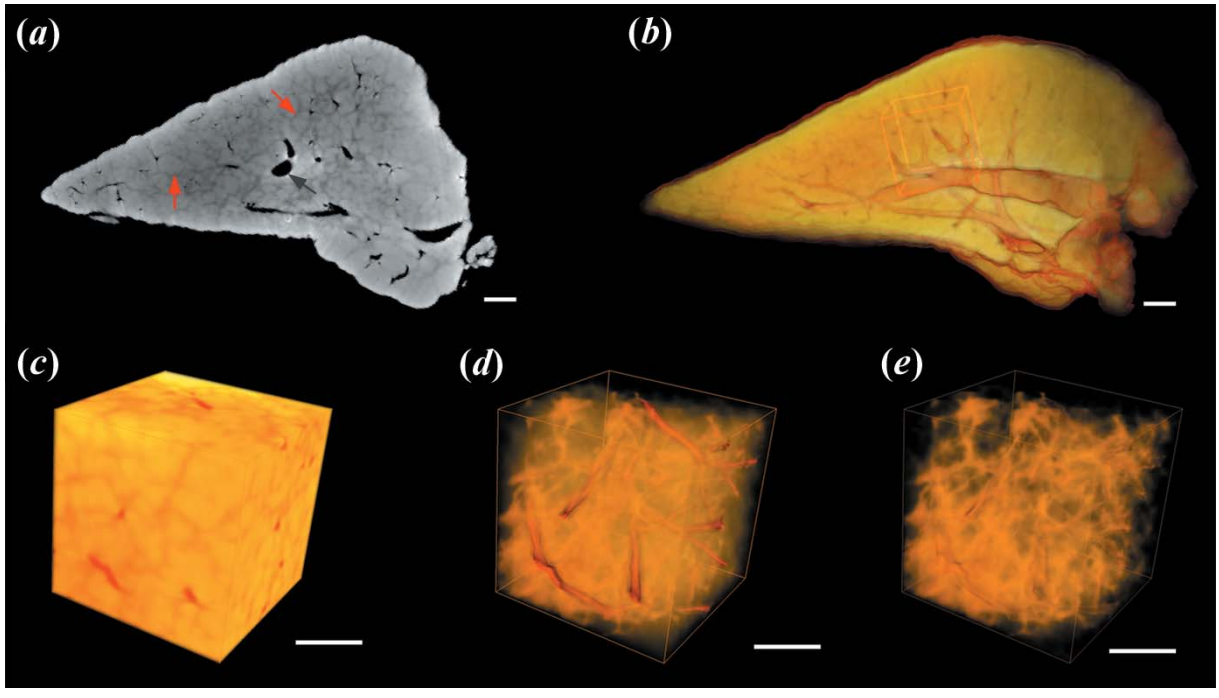

Figure 4
2D and 3D visualizations of the anatomical structures in a whole cirrhotic liver via PCCT. (*a*) CT slice. (*b*) 3D image of cirrhotic tissues. (*c*) Reconstruction of the box (200 × 200 × 200 pixels) in (*b*). (*d*) 3D visualization of fibrous tissues and vessels in (*c*). (*e*) Presentation of only the fibrous tissues in (*d*). Cirrhotic features are shown by red arrows (fibrous septa) and black arrows (vessels) in (*a*), and indicated in orange (fibrous tissues) and red (microvasculature) in the 3D images (*c*, *d* and *e*). Scale bar = 1 mm.

et al., 2014). PCCT is an emerging technique that provides excellent image contrast in soft-tissue imaging, and since this method has been developed many studies have used it to explore the microvasculature in liver disease (Duan *et al.*, 2013; Xuan *et al.*, 2015). Previous work has reported PCCT experiments on the fibrous tissues in liver fibrosis: the fibrous septa on the PCCT images were blurry, and their boundaries were indistinguishable (Fu *et al.*, 2016). Some studies have introduced the soft-tissue staining method into PCCT experiments to improve the collagen contrast, and the results showed that PCCT with iodine staining can clearly reveal the collagen structure in dermal tissues (Jiang *et al.*, 2012; Khonsari *et al.*, 2014). Thus, the method is applied in this study to explore the fibrous tissues in cirrhosis. The results showed that this approach prominently improves the image contrast of the fibrous structure compared with that achieved in the previous study (Fu *et al.*, 2016), and the 3D visualization of the fibrous tissues in cirrhosis was also possible due to the excellent image quality of this method, which indicated that PCCT with iodine staining has great potential for the characterization of cirrhosis.

Given the advantages of this approach, there are several potential applications of it in current experimental practice. Firstly, PCCT data can provide tomographic information of the samples at any angle, while histology offers 2D information in the cutting plane only. Some small injuries can be identified in time. Secondly, the *ex vivo* staining method is easy to handle, and the procedure does not impede further histological examinations. Unlike mechanical sectioning of the samples in traditional pathology, regions of interest can be located beforehand to aid the pathologist in producing true representative histological slices. Thirdly, this method allows for whole-volume imaging of the liver in rats, which is critical for the fibrosis structure in cirrhosis since it is a 3D network distributed in the liver. The 3D structures provide additional information for understanding the development of this disease, and the 3D quantitation of the fibrous tissues based on the 3D volume data is also feasible (Section S4 of the supporting information), contributing to a more comprehensive analysis of the disease. Besides the fibrous tissues, microvasculature was also clearly presented in the 3D images. The simultaneous presentation of 3D structures of the fibrous tissues and microvasculature offered a direct approach to studying the relation between these two structures during the development of cirrhosis. Finally, this approach can be extended to the analysis of other fibrotic diseases, but this requires further experimentation.

In terms of potential future implementation of PCCT, there are several limitations to this study. One main limitation of this study is using a synchrotron radiation source. High-quality images are obtained via use of the synchrotron radiation source; however, its size and cost do not allow this method to be widely transferred into laboratory practice. Recently, PCCT techniques with a conventional X-ray tube have been reported (Donath *et al.*, 2010; Hetterich *et al.*, 2014), which will be an important step in the evolution of PCCT towards its experimental and clinical implementation. Another main limitation is the long time interval (5 days) between preparation and scanning in this study, which could hinder the application of this method in *ex vivo* experiments. The preparation time selected in this primary experiment was to ensure that the liver was fully stained with iodine. Actually, several works have reported that the concentration of the solution also had a close relation to the image quality (Degenhardt *et al.*, 2010; Jeffery *et al.*, 2011). Thus, iodine staining with varying concentrations of iodine solution and less staining time will be evaluated in future studies to make this method more efficient in characterizing cirrhosis. Moreover, some studies reported that the soft-tissue samples were under slow rotation or kept on a horizontal shaking plate allowing for a smooth rocking during the sample preparation (Busse *et al.*, 2018; Dullin *et al.*, 2017), which might also facilitate penetration of the contrast agents to shorten the time.

In conclusion, compared with unstained PCCT, PCCT with iodine staining provides particularly higher imaging contrast for the detection of fibrous tissues and small nodules. The structures revealed by this approach are also highly consistent with the corresponding histological sections. Additionally, 3D visualization of these structures can be presented at the same time via this method. Although imperfect, this technique may serve as an adjunct nondestructive modality for 3D characterization of cirrhosis in an experimental setting.

Acknowledgements

The authors would like to thank the staff from beamline BL13W1 of SSRF, China, for their kind assistance in our experiments. All authors declare no conflict of interest.

Funding information

The following funding is acknowledged: National Natural Science Foundation of China (grant No. 81671683; grant No. 81670545; grant No. 81371549); WBE Liver Fibrosis Foundation of China (grant No. CFHPC20131033); Natural Science Foundation of Tianjin City in China (grant No. 16JCYBJC28600); Youth incubation fund of Tianjin Medical University General Hospital (grant No. ZYYFY2016015).

References

Albers, J., Pacilé, S., Markus, M. A., Wiart, M., Vande Velde, G., Tromba, G. & Dullin, C. (2018). *Mol. Imaging Biol.* **20**, 732–741.
Anthony, P. P., Ishak, K. G., Nayak, N. C., Poulsen, H. E., Scheuer, P. J. & Sobin, L. H. (1978). *J. Clin. Pathol.* **31**, 395–414.
Busse, M., Müller, M., Kimm, M. A., Ferstl, S., Allner, S., Achterhold, K., Herzen, J. & Pfeiffer, F. (2018). *Proc. Natl Acad. Sci. USA*, **115**, 2293–2298.
Cárdenas, A. & Ginès, P. (2009). *Curr. Opin. Gastroenterol.* **25**, 195–201.
Chen, R.-C., Dreossi, D., Mancini, L., Menk, R., Rigon, L., Xiao, T.-Q. & Longo, R. (2012). *J. Synchrotron Rad.* **19**, 836–845.
Chen, R. C., Rigon, L. & Longo, R. (2011). *J. Phys. D Appl. Phys.* **44**, 495401.

Constandinou, C., Henderson, N. & Iredale, J. P. (2005). *Methods Mol. Med.* **117**, 237–250.
Degenhardt, K., Wright, A. C., Horng, D., Padmanabhan, A. & Epstein, J. A. (2010). *Circ. Cardiovasc. Imaging*, **3**, 314–322.
Donath, T., Pfeiffer, F., Bunk, O., Grünzweig, C., Hempel, E., Popescu, S., Vock, P. & David, C. (2010). *Invest. Radiol.* **45**, 445–452.
Duan, J., Hu, C., Luo, S., Zhao, X. & Wang, T. (2013). *PLoS One*, **8**, e78176.
Dullin, C., Ufartes, R., Larsson, E., Martin, S., Lazzarini, M., Tromba, G., Missbach-Guentner, J., Pinkert-Leetsch, D., Katschinski, D. M. & Alves, F. (2017). *PLoS One*, **12**, e0170597.
Fitzgerald, R. (2000). *Phys. Today*, **53**, 23–26.
Fu, Y., Peng, H. J., Zhang, X., Peng, W. J., Wu, J., Wang, S. P., Du, M. & Li, R. M. (2016). *Eur. Radiol.* **26**, 2947–2955.
Geith, T., Brun, E., Mittone, A., Gasilov, S., Weber, L., Adam-Neumair, S., Bravin, A., Reiser, M., Coan, P. & Horng, A. (2018). *Am. J. Roentgenol.* **210**, 1317–1322.
Gerneke, D. A., Sands, G. B., Ganesalingam, R., Joshi, P., Caldwell, B. J., Smaill, B. H. & Legrice, I. J. (2007). *Microsc. Res. Tech.* **70**, 886–894.
He, Y., Kang, C. H., Xu, S., Tuo, X., Trasti, S., Tai, D. C., Raja, A. M., Peng, Q., So, P. T., Rajapakse, J. C., Welsch, R. & Yu, H. (2010). *J. Biomed. Opt.* **15**, 056007.
Hetterich, H., Willner, M., Fill, S., Herzen, J., Bamberg, F., Hipp, A., Schüller, U., Adam-Neumair, S., Wirth, S., Reiser, M., Pfeiffer, F. & Saam, T. (2014). *Radiology*, **271**, 870–878.
Holdsworth, D. W. & Thornton, M. M. (2002). *Trends Biotechnol.* **20**, S34–S39.
Hu, J., Ni, S., Cao, Y., Wang, X., Liao, S. & Lu, H. (2017). *Spine*, **42**, E883–E889.
Jeffery, N. S., Stephenson, R. S., Gallagher, J. A., Jarvis, J. C. & Cox, P. G. (2011). *J. Biomech.* **44**, 189–192.
Jiang, Y., Tong, Y. & Lu, S. (2014). *J. Tissue Eng. Regen. Med.* **8**, 794–800.
Jiang, Y., Tong, Y., Xiao, T. & Lu, S. (2012). *Dermatology*, **225**, 75–80.
Khonsari, R. H., Healy, C., Ohazama, A., Sharpe, P. T., Dutel, H., Charles, C., Viriot, L. & Tafforeau, P. (2014). *Anat. Rec.* **297**, 1803–1807.
Lin, J., Lu, F., Zheng, W., Xu, S., Tai, D., Yu, H. & Huang, Z. (2011). *J. Biomed. Opt.* **16**, 116024.
Metscher, B. D. (2009*a*). *BMC Physiol.* **9**, 11.
Metscher, B. D. (2009*b*). *Dev. Dyn.* **238**, 632–640.
Missbach-Guentner, J., Pinkert-Leetsch, D., Dullin, C., Ufartes, R., Hornung, D., Tampe, B., Zeisberg, M. & Alves, F. (2018). *Sci. Rep.* **8**, 1407.
Mohun, T. J. & Weninger, W. J. (2011). *Curr. Opin. Genet. Dev.* **21**, 573–578.
Momose, A. (2005). *Jpn J. Appl. Phys.* **44**, 6355–6367.
Ntziachristos, V. (2010). *Nat. Methods*, **7**, 603–614.
Ourselin, S., Roche, A., Subsol, G., Pennec, X. & Ayache, N. (2001). *Image Vis. Comput.* **19**, 25–31.
Soresi, M. (2014). *World J. Gastroenterol.* **20**, 18131–18150.
Sun, T. L., Liu, Y., Sung, M. C., Chen, H. C., Yang, C. H., Hovhannisyan, V., Lin, W. C., Jeng, Y. M., Chen, W. L., Chiou, L. L., Huang, G. T., Kim, K. H., So, P. T., Chen, Y. F., Lee, H. S. & Dong, C. Y. (2010). *J. Biomed. Opt.* **15**, 036002.
Thabut, D. & Shah, V. (2010). *J. Hepatol.* **53**, 976–980.
Weitkamp, T., Haas, D., Wegrzynek, D. & Rack, A. (2011). *J. Synchrotron Rad.* **18**, 617–629.
Winklhofer, S., Peter, S., Tischler, V., Morsbach, F., von Werdt, M., Berens, S., Modregger, P., Buser, L., Moch, H., Stampanoni, M., Thali, M., Alkadhi, H. & Stolzmann, P. (2015). *Radiology*, **277**, 64–72.
Xie, H., Deng, B., Du, G., Fu, Y., He, Y., Guo, H., Peng, G., Xue, Y., Zhou, G., Ren, Y., Wang, Y., Chen, R., Tong, Y. & Xiao, T. (2013). *J. Instrum.* **8**, C08003.
Xu, S., Wang, Y., Tai, D. C. S., Wang, S., Cheng, C. L., Peng, Q., Yan, J., Chen, Y., Sun, J., Liang, X., Zhu, Y., Rajapakse, J. C., Welsch, R. E., So, P. T. C., Wee, A., Hou, J. & Yu, H. (2014). *J. Hepatol.* **61**, 260–269.
Xuan, R., Zhao, X., Hu, D., Jian, J., Wang, T. & Hu, C. (2015). *Sci. Rep.* **5**, 11500.